Separation and Purification Technology 298 (2022) 121447

Contents lists available at ScienceDirect

Separation and Purification Technology

journal homepage: www.elsevier.com/locate/seppur

PIM-1 membranes containing POSS - graphene oxide for CO_2 separation

Sajjad Mohsenpour [a], Ahmed W. Ameen [a], Sebastian Leaper [a], Clara Skuse [a], Faiz Almansour [a], Peter M. Budd [b], Patricia Gorgojo [a,c,d,*]

[a] Department of Chemical Engineering, Faculty of Science and Engineering, The University of Manchester, Manchester M13 9PL, UK
[b] Department of Chemistry, Faculty of Science and Engineering, The University of Manchester, Manchester M13 9PL, UK
[c] Instituto de Nanociencia y Materiales de Aragón (INMA) CSIC-Universidad de Zaragoza, C/ Mariano Esquillor s/n, 50018 Zaragoza, Spain
[d] Departamento de Ingeniería Química y Tecnologías del Medio Ambiente, Universidad de Zaragoza, C/ Pedro Cerbuna 12, 50009 Zaragoza, Spain

ARTICLE INFO

Keywords:
Graphene Oxide
POSS, PIM-1 membrane
Mixed matrix membrane
CO_2 separation

ABSTRACT

PIM-1 mixed matrix membranes (MMMs) were fabricated with polyhedral oligomeric silsesquioxane (POSS) and graphene oxide (GO) functionalized with POSS (GO-POSS), and tested for CO_2/N_2 (single gas) and CO_2/CH_4 (1:1, v:v gas mixture). The CO_2 permeability of the best performing fresh MMM (containing 0.05 wt% GO-POSS) was ~ 12000 Barrer, which is 69% higher than that of the neat PIM-1 membrane, with about the same selectivity (CO_2/CH_4 selectivity ~ 12 and CO_2/N_2 selectivity ~ 20). In both cases, the gas separation data surpass the 2008 Robeson upper bound. In addition to the initial CO_2 permeability enhancement, the use of GO-POSS is an efficient strategy to slow down physical aging. The MMM at a filler loading of 0.75 wt% showed less than half of the reduction in CO_2 permeability than the neat PIM-1 membrane 160 days after preparation (26% for the MMM vs 58% for the purely polymeric one).

1. Introduction

It has been widely accepted that the release of greenhouse gases such as carbon dioxide (CO_2) into the atmosphere from human activities is a major contributor to climate change. This in turn can increase the frequency and severity of extreme weather events such as heatwaves, floods and droughts [1]. According to the 2015 Paris agreement, global warming must be kept below 1.5 °C to prevent catastrophic effects [2]. One strategy to achieve this is to capture CO_2 from the atmosphere or directly from industrial processes using carbon capture and storage (CCS) technologies. However, these are currently expensive and energy intensive [3]. CO_2 presents additional problems for the production of electricity from lower-emission energy sources such as natural gas and biogas (which are mostly CH_4). Both natural gas and biogas contain CO_2 (2–50%) which must be removed because it is corrosive to gas pipelines and reduces the calorific value of the fuel [4]. Therefore, there is an immediate need for technologies that can separate CO_2 from methane (CH_4) and air (nitrogen (N_2)). The adoption of polymeric gas separation membranes has grown within industrial applications due to their low cost, good processability and ease of fabrication [5]. However, the trade-off between selectivity and permeability is the major drawback of the polymeric membranes, holding back their wider use for these applications.

Polymers of intrinsic microporosity (PIMs) are superglassy polymers with high free volume that have attracted considerable attention as membrane materials for gas separations over the past two decades [6-10]. PIM-1, the most studied PIM, has high CO_2 permeability and is soluble in a few common organic solvents, including chloroform and tetrahydrofuran (THF), which allows for the fabrication of dense membranes via casting and solvent-evaporation. Physical aging and plasticization in high free-volume membranes are the main limiting factors when it comes to real-life applications. Aging is caused by the relaxation of the non-equilibrium polymer chains and results in free-volume collapse and substantial gas permeability decrease over time. The so-called plasticization, on the other hand, is caused by the sorption of condensable gases at high pressures that induces swelling, and leads to decreased selectivity [11]. To minimize aging and plasticization, different approaches have been proposed including polymer structure modification, crosslinking and addition of non-porous and microporous fillers (mixed matrix membranes (MMMs)) [12]. Rational selection of the filler with an appropriate structure (particle size, pore orientation, etc.) and resistance to aggregation (i.e. minimization of the interfacial

* Corresponding author at: Departamento de Ingeniería Química y Tecnologías del Medio Ambiente, Universidad de Zaragoza, C/ Pedro Cerbuna 12, 50009 Zaragoza, Spain.
E-mail address: pgorgojo@unizar.es (P. Gorgojo).

https://doi.org/10.1016/j.seppur.2022.121447
Received 29 April 2022; Received in revised form 4 June 2022; Accepted 5 June 2022
Available online 15 June 2022

incompatibility between the filler and the polymer) is crucial to obtain MMMs with superior properties [13]. Porous aromatic frameworks (PAFs) [14], carbon nanotubes (CNTs) [15], polyhedral oligomeric silsesquioxane (POSS) [11,16], graphene [17-19], and metal organic frameworks (MOFs) [20] are some examples of filler that have been used for the preparation of PIM-1-based MMMs.

Graphene oxide (GO) derivatives have been used as fillers in PIM-1 and other polymer matrices due to their high aspect ratio (>1000), high stability and abundant functional groups in GO for surface functionalization [21]. When GO flakes are dispersed in common organic solvents (such as those used to dissolve PIM-1) they do not form a stable colloidal suspension, and thus GO functionalization is needed. Our research group incorporated in a previous work octylamine (OA) and octadecylamine (ODA)- functionalized GO into PIM-1 membranes and slower rates of aging were reported [18]. This was due to the large lateral flake size of the functionalized GO, which induced rigidification of PIM-1 polymer chains. However, CO_2 permeability decreased with the addition of the fillers for freshly-prepared membranes, as a consequence of the non-porous nature of GO (i.e. increased tortuosity = increased path length of diffusing gas molecules). Work on the incorporation of other functionalized GO materials: (PIM-1)-functionalized (3-aminopropyl)triethoxysilane GO (APTS-GO) [19] and (PIM-1)-functionalized holey GO [22] followed, but decrease CO_2 permeability for non-aged membranes as compared to neat PIM-1 was also observed.

To overcome the reduction in gas permeability, we present in this work the decoration of GO nanosheets with porous nanoparticles (NPs) that can create additional gas transport channels and still aid in reducing the physical aging in PIM-1 matrices. Porous aminopropyl isobutyl POSS NPs (AM0265, referred to here as POSS) anchored to GO and as received (without GO) have been used as fillers in PIM-1 membranes. Unlike GO, the POSS and the GO-POSS NPs (with a cage-like three-dimensional structure of 1–3 nm in size [23,24] and chemical structure shown in Figure S1) can both be dispersed in chloroform and THF, which are the organic solvents used to dissolve PIM-1. The high aspect ratio of the GO-POSS is expected to increase the interaction with the polymer chains, and thus aid in suppressing the physical aging phenomena while maintaining a high gas separation performance.

2. Experimental

2.1. Materials

PIM-1 polymer was synthesized with monomers of 3,3,3′,3′-tetramethyl-1,1′-spirobisindane-5,5′,6′,6′-tetrol, 97% (TTSBI, Alfa Aesar (UK)) and 2,3,5,6-tetrafluoroterephthalonitrile, 99% (TFTPN, Fluorochem Ltd.). TTSBI was used after a purification step. For this, 15 g TTSBI was dissolved in 400 ml methanol (MeOH) (VWR International Ltd) and the temperature was increased to 120 °C while stirring the solution in an open beaker until 300 ml of MeOH had evaporated. Then 200 ml dichloromethane (DCM) (Sigma Aldrich, UK) was added to the beaker and the precipitate was filtered and dried under vacuum (10 mbar) at 50 °C for 5 h (~60% yield). Potassium carbonate (K_2CO_3) was purchased from Fisher Scientific UK Ltd. Both K_2CO_3 and TFTPN were dried in the vacuum oven at 25 °C overnight prior to use. Chloroform was provided by Fisher Chemical. N,N-dimethylacetamide (DMAc), toluene, and 1,4-dioxane were purchased from Sigma Aldrich (UK). Acetone was purchased from VWR International Ltd. Deionized water (DI) used in this study was produced by a Milli-Q integral system (Merck Millipore, Ireland).

For GO functionalization with POSS, GO (1 wt% aqueous suspension) was purchased from William Blythe (Lancashire, UK), POSS powder was purchased from Hybrid Plastics (US), N,N'-dicyclohexylcarbodiimide (DCC), and tetrahydrofuran (THF) were purchased from Sigma Aldrich (Germany).

2.2. PIM synthesis

PIM-1 synthesis was based on the procedure described in the work by Ameen et al. [7]. Briefly, TTSBI (10.79 g, 0.031 mol), TFTPN (6.26 g, 0.031 mol), anhydrous K_2CO_3 (12.85 g, 0.093 mol), DMAc (60 ml) and toluene (30 ml) were added to a three neck round bottom flux and reacted under a continuous flow of dry N_2 using a mechanical stirrer at 160 °C. At the end of the reaction (after 36 min), the solution was added to MeOH to precipitate out the PIM-1, which was filtered, dried and re-dissolved in 300 ml chloroform overnight and subsequently re-precipitated using MeOH. The resulting polymer was washed with DI water overnight and subsequently with 1,4-dioxane, acetone, and MeOH. Finally, PIM-1 was dried in a vacuum oven at 120 °C for 2 days (yield ~ 95%).

2.3. Graphene oxide-POSS functionalization

POSS functionalized GO was synthesized according to the method described by Xue et al. [25] 100 mg dried GO was dispersed in 50 ml of THF using a sonication bath (Elmasonic, 80 kHz frequency at 100% power) for 2 h. This was transferred to a 250 ml round bottom flask along with 2 g POSS and 100 mg DCC and sonicated for another 10 min, and then refluxed at 80 °C for 48 h. At the end of the reaction, the solution was poured into MeOH (500 ml). The precipitate was collected by vacuum filtration (homemade polyacrylonitrile filter (0.2 μm pore size)). The filtration procedure was repeated several times to remove unreacted POSS from the final filter powder (Figure S2) and the obtained powder was labelled GO-POSS48. In order to synthesise GO-POSS with higher POSS content, the functionalization reaction was repeated with higher initial POSS content (4 g) and longer reaction time (72 h), and the obtained powder was labelled GO-POSS72. The schematic of GO functionalization with POSS is shown in Figure S1. In contrast to GO, GO-POSS is soluble in chloroform (Figure S3).

2.4. Membrane fabrication

To prepare the MMMs, first a GO-POSS/chloroform solution (0.8 mg ml^{-1}) was prepared using a sonication bath (80 kHz frequency at 100% power) for 2 h. Aliquots of this solution were diluted with chloroform (total volume 4.5 ml) and stirred for 1 h. Following this, 0.14 g of PIM-1 powder was dissolved in each solution. The obtained solutions were stirred for 6 h, followed by 10 min sonication. Immediately after the sonication, the solutions were filtered through glass wool (Sigma Aldrich) and cast in 5 cm petri dishes. To reduce the solvent evaporation rate, the petri dishes were covered with a glass lid with a minimal gap and left in a fume cupboard to dry at room temperature for 18 h. Then, the solidified membranes were soaked in MeOH for 8 h and subsequently dried under vacuum (10 mbar) at 65 °C overnight (~12–14 h). MeOH treatment helps to remove the chloroform residue and increases the fractional free volume (FFV) and gas permeability [26]. The residue of solvent in the membrane affects its performance and it is much easier to remove MeOH from the polymer matrix than chloroform [27]. The PIM-1 membranes prepared with GO-POSS48 and GO-POSS72 were labelled 48PGP(x) and 72PGP(x), respectively where x (=0.01, 0.05, 0.1, 0.25, 0.5, 0.75) referred to the percentage (wt%) of GO-POSS to PIM-1, and *PGP* are the initials in PIM-1/GO-POSS. In addition, to study the role of potentially available oxygen functional groups of GO on the gas separation performance, GO-POSS72 was reduced at 120 °C for 8 h following the procedure as described in a previous publication [28] and labelled rGO-POSS72. A digital photo of rGO-POSS72 dispersed in chloroform is shown in Figure S3. The MMMs prepared by this filler were labelled PrGP(x) (x = 0.01, 0.05 and 0.1 wt%).

Purely polymeric and PIM-1 membranes with only POSS (no GO) were also prepared and used as the control membranes. They were prepared following the same procedure as for the PGP membranes described in the previous paragraph, and were labelled PP(x) (x = 0.02,

0.03, 0.05, 2, 5 wt%). It should be noted that GO or rGO could not be homogeneously dispersed in chloroform so they were not used as a filler.

The thicknesses of the membranes were measured using a digital micrometer (Mitutoyo Corporation) with an accuracy of ± 0.5 μm. For each membrane, 3–5 measurements were carried out and the average results are reported in Figure S4. In order to preserve the integrity of the membranes and be able to retest for gas separation after several weeks/months, membrane discs were sandwiched between two circular pieces of aluminium with concentric circular holes and sealed with epoxy resin (Araldite Rapid, Industrial MTCE Suppliers). The effective membranes areas available for gas permeation after the sealing were calculated by ImageJ software and were ~ 0.1 cm^2.

2.5. Materials and membranes characterization

2.5.1. PIM-1 polymer characterization

The molecular weight of the synthesized PIM-1 polymer was measured using gel permeation chromatography (GPC, Viscotek GCPmax VE 2001 chromatograph (Malvern, UK)) [29]. The results were analyzed by OmniSEC software. ^{1}H Nuclear Magnetic Resonance (H-NMR) spectroscopy was performed using a Bruker DPX 400 MHz spectrometer. Matrix assisted laser desorption/ionization-time of flight (MALDI-TOF) mass spectroscopy was carried out on a Shimadzu Biotech Axima Confidence instrument. Nitrogen adsorption isotherms were acquired using a Micromeritics ASAP 2020 sorption analyzer according to the procedure reported by Ameen et al. [7].

2.5.2. Characterization of fillers and membranes

The functionalization of GO with POSS was evaluated through a range of characterization techniques: X-ray photoelectron spectroscopy (XPS), attenuated total reflectance Fourier transform infrared (ATR-FTIR) spectroscopy, X-Ray diffraction (XRD), thermogravimetric analysis (TGA), atomic force microscopy (AFM) and scanning and transmission microscopies. Some of these techniques (XRD, TGA and scanning electron microscopy (SEM)) were also used for the characterization of the prepared membranes.

XPS was conducted using an Axis Ultra spectrometer (Kratos Analytical Limited, Manchester, UK) with a monochromatic Al Kα source (1486.7 eV). ATR-FTIR was carried out in an iDS Nicolet iS5 spectrometer (Thermo Scientific, UK) with a wavenumber range of 400–4000 cm^{-1}. XRD measurements were carried out to analyse the interlayer space (*d*-spacing) of GO and GO-POSS, according to Bragg's law (equation (1)) [30], and also to investigate the crystallinity of the prepared membranes. Samples were measured in a PANalytical X'Pert Pro equipment with Cu Kα and Kβ emission lines in a 2 θ range of 4°-50°.

$$d = \frac{\lambda}{2sin\theta} \tag{1}$$

where λ is the wavelength of the X-ray beam (0.154 nm in this equipment) and θ (degree) is the diffraction angle.

A TGA550 thermal analyser (TA Instruments) was utilized to study the chemical functionalization of GO-POSS and the thermal stability of the fillers and the MMMs. The analyses were performed at a heating rate of 10 °C min^{-1} under N_2 flow from 40 to 800 °C.

The average size of GO-POSS flakes was measured using SEM (FEI Quanta 250 FEG-SEM). Transmission electron microscopy (TEM, FEI Tecnai G2 20) was conducted to investigate structural features of GO and GO-POSS flakes. The samples were prepared by drop-casting on a lacey carbon film on a 200 mesh copper grid (Agar Scientific). In addition, the thickness and surface morphology of GO and GO-POSS nanosheets were assessed using an AFM. The samples were prepared by drop-casting 30 μl of a 100 ppm GO-POSS solution on clean mica substrates.

To study the morphology of prepared membranes, cross-sectional and surface SEM images were taken using an FEI Quanta 650 SEM.

2.6. Gas separation performance

Single gas separation tests were conducted for different gas molecules including H_2, CO_2, CH_4, and N_2 using the constant-pressure variable volume method. The permeate gas composition was analyzed using a gas chromatograph column (Agilent 490 microGC) which has two channels, a molecular sieve (MS) and a PoraPlotU (PPU) column. H_2 and N_2 were quantified from the peaks obtained in the MS, and the CH_4 and CO_2 permeability from the peaks in the PPU. Mixed gas separations were also carried out in the same setup, but feeding a mixture (CO_2/CH_4 at 50:50 vol%) into the membrane cell. For CO_2/N_2 separation, single-component gases were used. The transmembrane pressure was ~ 1 bar and the membranes were placed inside an oven at a constant temperature of 25 °C. Argon (Ar) or helium (He) were used to sweep the permeate gas and send it to the MS and the PPU channels, respectively. The feed and sweep gas flow rates were 80 ml min^{-1} and 10 ml min^{-1}, respectively, to maintain the stage cut ($\frac{\text{permeate flow}}{\text{feed flow}}$) always below 2 wt% and constant feed composition. More details on the gas separation unit can be found elsewhere [7]. The gas permeability was calculated according to the following equation:

$$P_i = \frac{Q_i L}{A(y_i p_f - x_i p_p)} \times 10^{10} \tag{2}$$

where, P_i is the permeability in Barrer unit (1 Barrer = 10^{-10} cm^3 (STP) cm cm^{-2} s^{-1} $cmHg^{-1}$), Q_i (cm^3 s^{-1}) is the gas flow rate of component *i*, *L* (cm) is the membrane thickness, *A* (cm^2) is the effective membrane area. p_f and p_p (cmHg) are the total pressures in the feed and permeate side, respectively. y_i and x_i are the mole fraction of component *i* in the feed and the permeate side, respectively.

The selectivity (α) was calculated by dividing the permeability of gas A (which shows higher permeability) by the permeability of gas B according to equation (3).

$$\alpha_{A/B} = \frac{P_A}{P_B} \tag{3}$$

For each membrane variant, 3 to 5 samples were prepared and average results along with the standard deviations have been reported. The tested fresh membranes were stored in a sealed petri dish. 48GP MMMs were re-tested after 7, 21, 55, 125, and 160 days and 72PGP MMMs were retested after 110 and 160 days in order to evaluate the physical aging. The CO_2 permeability drop and relative CO_2 permeability were calculated according to equations (4) and (5).

$$\text{Permeability drop} = P_{CO_2}^{fresh} - P_{CO_2}^{aged} \tag{4}$$

$$\text{Relative } P_{CO_2} = \frac{P_{CO_2}^{aged}}{P_{CO_2}^{fresh}} \tag{5}$$

To obtain more insight into the role of GO-POSS in the PIM-1 membranes, the diffusion coefficient (*D*, cm^2 s^{-1}) and solubility (*S*, cm^3 (STP) cm^{-3}.$cmHg^{-1}$) for CO_2 and CH_4 in selected MMMs and pristine PIM-1 membranes were obtained using a time-lag apparatus (constant-volume variable pressure method) at ambient temperature (~20 °C) and a feed pressure of 1.2 bar. The apparatus is described in more detail elsewhere [7]. The permeability (P_i(Barrer)) can be calculated by equations (6) and (7) and *D* and *S* were calculated with equations (8) and (9), respectively.

$$Q_i = \frac{V_p \vartheta_{STP} \theta_i}{RT} \tag{6}$$

$$P_i = \frac{Q_i L}{A\Delta p} \times 10^{10} \tag{7}$$

$$D_i = \frac{L^2}{6\tau_i} \tag{8}$$

$$S_i = \frac{P_i}{D_i} \tag{9}$$

where, V_p (53.68 cm^3) is the permeate side volume, ϑ_{STP} (22400 cm^3 mol^{-1}) is the molar volume of the gas at standard temperature and pressure. R (6236.36 cmHg.cm^3 K^{-1}.mol^{-1}) is gas constant and T (K) is the absolute temperature. Δp (cmHg) is the average transmembrane pressure. L (cm) is the membrane thickness, θ_i (cmHg s^{-1}) is the build-up of permeate side pressure and τ_i (s) is time-lag which has been obtained from the permeate side pressure vs time graph.

In this study, the permeability of the prepared MMMs was modelled using Maxwell-Wagner-Sillars equation (equation (10)).

$$P_{MMMs} = P_c\left[\frac{nP_d + (1-n)P_c - (1-n)(P_c - P_d)\varnothing_f}{nP_d + (1-n)P_c + n(P_c - P_d)\varnothing_f}\right] \tag{10}$$

where,P_{MMMs} is the predicted permeability in Barrer. P_c is the permeability of the continuous phase ($P_{PIM\text{-}1}$, Barrer), P_d is the permeability of the dispersed phase ($P_{GO-POSS}$, Barrer) and $\varnothing_f$ denotes the fractional volume of the dispersed phase. n is the filler shape factor ranging from 0 to 1. For prolate ellipsoids $0 \leq n \leq 1/3$ and for oblate ellipsoids $1/3 \leq n \leq 1$. When the value of n is assumed 1/3 it means the fillers are spherical and equation (10) is known as the Maxwell equation. The limits of $n = 0$ and $n = 1$ represent the permeation of gas through parallel plates (horizontal) and laminate series plates (vertical), respectively [31].

This simple model has been widely applied for the prediction of permeation performance for membranes at low particle loadings (volume fraction $\leq$ 0.2) [31], and it has been successfully used for membranes containing 2D fillers [7]. To convert the mass fraction of the dispersed phase to the volume fraction, densities of PIM-1, GO and POSS were considered 1.1, 1.8 and 1.2 g cm^{-3}, respectively. The reported permeance of a 50 nm thick GO-POSS laminate membrane is 35 GPU [32]. That gives a permeability value of 1.75 Barrer, which is much lower than that of the PIM-1 membrane and can therefore be neglected.

3. Results and discussion

3.1. PIM-1 characterization

The synthesized PIM-1 exhibited a weight-average molar mass (M_w) and number-average molar mass (M_n) of 153000 g mol^{-1} and 67500 g mol^{-1}, respectively, with dispersity (M_w/M_n) of 2.26. The BET surface area was 756 m^2 g^{-1} according to the N_2 adsorption isotherms (Figure S5 of the supporting information), which is in agreement with the range reported in the literature (400–800 m^2 g^{-1}) [33].

The ^{1}H NMR spectrum of the PIM-1 powder is shown in Figure S6, and the structure of the PIM-1 polymer is discussed in the supporting information. The ^{1}H NMR shows that the synthesized polymer has a proportion of branched structure. Figure S7 displays the MALDI TOF mass analysis of the synthesized PIM-1, which confirms its cyclic structure at low molar mass. The fragmentation product peaks are also observed which may originate from the presence of the branched structure that is consistent [7] with the ^{1}H NMR results. The weight percentages of carbon (C) and nitrogen (N) for the synthesized PIM-1 are 74.19 and 6.11, respectively with C/N ratio of 12.14, which is slightly lower than the theoretical value of C/N for a typical PIM-1 (12.43). This may be the result of the presence of the polymer structures terminated with a fluoro monomer (which has nitrogen in its structure) [34].

3.2. GO-POSS characterization

Unlike GO, the prepared GO-POSS samples can be dispersed in chloroform (pictures in Figure S3). XPS confirms the presence of silicon and nitrogen elements for the GO-POSS nanohybrids; Si 2p, Si 2 s and nitrogen peaks are identified in the XPS survey of GO-POSS72 (Figure S8b) at 99.5, 150 and 399.5 eV, respectively. Furthermore, the high-resolution spectra of N 1 s for GO-POSS72 (Fig. 1a) and GO-POSS48 (Figure S8d) show a peak at 399.9 eV that corresponds to amide bonds (O = C –NH) [32,35,36], and confirms covalent bond formation between GO and POSS (see proposed molecular model in Figure S1). The high-resolution spectrum of C 1 s for GO-POSS72 (Fig. 1b) shows a peak at 285.3 eV that corresponds to C-N [37-39], which is not found for GO (C1s spectrum in Figure S8e) and is further evidence of POSS presence in the prepared GO-based nanohybrids.

The oxygen-containing functional groups in GO (carboxylic and epoxy groups) provide sites for the nucleophilic substitution reaction with amine groups in POSS. Therefore, the decline in oxygen percentage of GO-POSS in comparison with GO (atomic percentage values are shown in Table S1 of the supporting information) can be attributed to the chemical functionalization between amine and oxygen functional groups, as shown by the presence of amide bonds in the N 1 s spectra and as reported in other studies [40-42]. Some of the oxygen loss may be also ascribed to partial reduction of the GO at 80 °C (temperature of GO-POSS functionalization reaction). The higher Si and N content in the GO-POSS72 sample as compared to GO-POSS48 suggests higher POSS concentration at longer reaction times. FTIR spectra (Figure S9) are consistent with XPS results.

The average interlayer distance of GO and GO-POSS nanosheets was calculated from the XRD data (Fig. 1c) using Bragg's law (equation (1)); the characteristic broad GO peak at 11.5° gives a d-spacing of 0.77 nm, in agreement with reported values in the literature for GO [43]. For the GO-POSS nanohybrids the characteristic GO peak broadens and decreases its intensity, shifting to lower 2θ values of 10.1° (d-spacing = 0.87 nm) and 9.1° (d-spacing = 0.97 nm) upon functionalization for 48 h (GO-POSS48) and 72 h (GO-POSS72), respectively. The increase in the interlayer space upon reaction suggests that covalently-bonded POSS moieties have been intercalated between the GO sheets, as reported elsewhere [25]. However, the higher increase in the interlayer space for GO-POSS72 is accompanied by a lower crystallinity, suggesting that longer reaction times lead to a more disordered structure. It is also worth noting that the characteristic (0 0 2) peak at $2\theta \sim 25°$ that is normally reported upon reduction of GO is not observed for the GO-POSS nanohybrids (nor for the reduced sample rGO-POSS72), which further confirms successful intercalation of POSS, rather than reduction, at the reaction conditions.

The TGA curves of GO and GO-POSS samples are shown in Fig. 1d. The GO weight reduced by ~10% up to 100 °C due to desorption of adsorbed water molecules, while no significant loss was detected for GO-POSS48 and GO-POSS72 because of their hydrophobic nature. For GO, significant weight losses in the range of 180–240 °C and above 550 °C were observed and ascribed to decomposition of oxygen functional groups and the graphite skeleton, respectively [19]. GO-POSS showed better thermal stability than POSS, which decomposes completely at ~300 °C. The thermal stability for GO is also improved after the reaction with POSS (final weight for GO at 800 °C ~ 2 wt% and > 40 wt% for the GO-POSS samples) as amide bonds in GO-POSS prevent thermal degradation of the GO carbon skeleton [25,37]. The higher final weight percentage of GO-POSS72 than GO-POSS48 at 800 °C (46 and 40 wt%, respectively) suggests a slightly higher degree of functionalization (i.e. more amide bonds) for the sample obtained after reaction with 72 h.

The average flake size of GO-POSS (0.79 ± 0.32 μm) was calculated using Gaussian curve fitting from SEM images (Figure S10). The structural properties and height profile of GO and GO-POSS have been studied by AFM and TEM and some images are shown in Figures S 11&12. The higher height profiles for GO-POSS72 (Figure S11b) and GO-POSS48 (Figure S11c) as compared to the one for GO (Figure S11a) also confirm the presence of POSS on GO for GO-POSS samples.

3.3. Membrane characterization

FTIR was used to study the possible interaction of the fillers (GO-

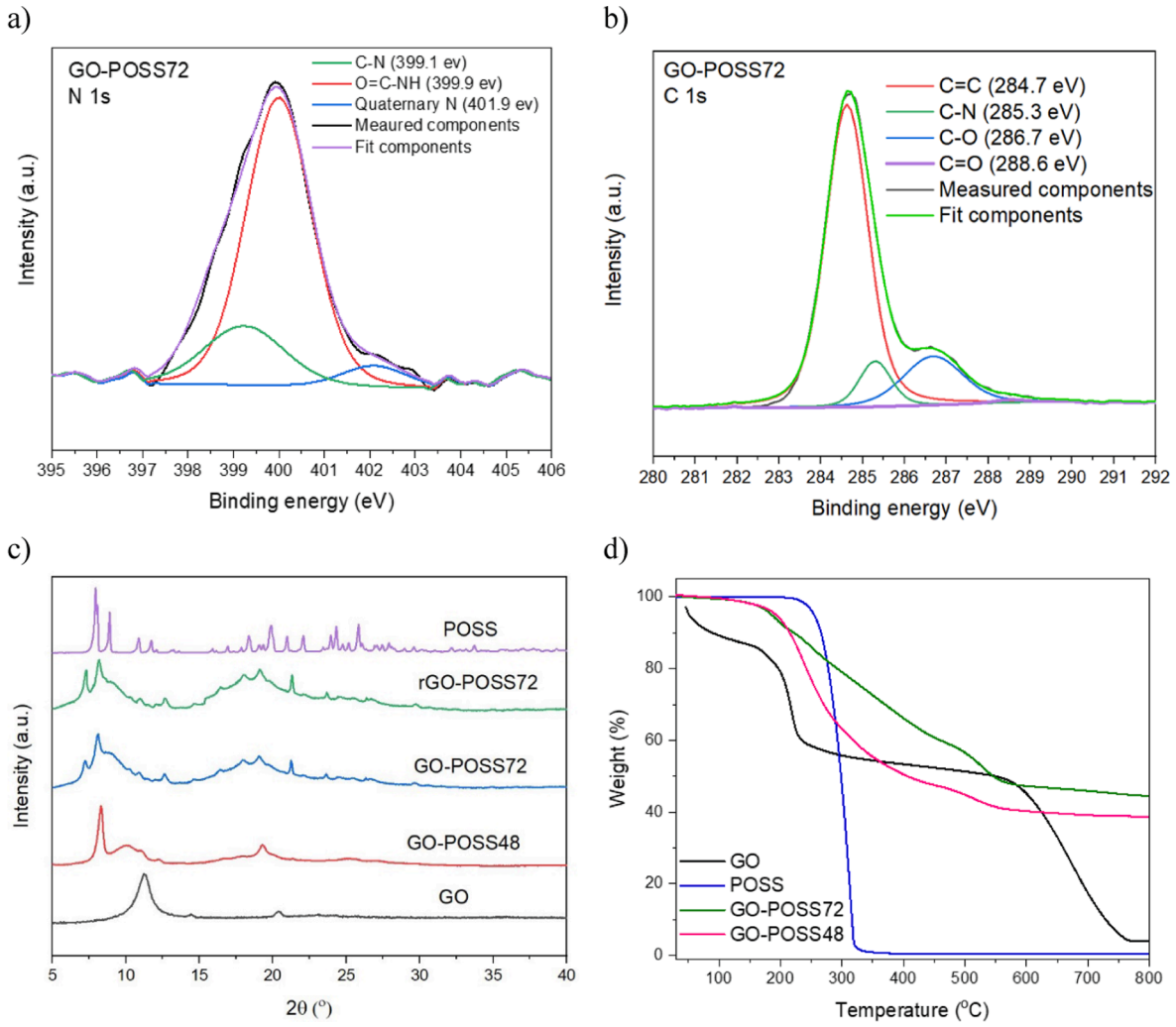

Fig. 1. High-resolution spectra of N 1s (a) and C 1s (b) for GO-POSS72, normalized XRD spectra (c) and TGA curves (d) of GO, POSS, GO-POSS48, and GO-POSS72. The XRD spectrum of the reduced sample rGO-POSS72 is also included in (c).

POSS and POSS) and the PIM-1 polymer (Figure S13). The amide groups in GO-POSS and amine groups in POSS have –NH bonds in their structures which can form hydrogen bonds with cyano (-C≡N) groups in the PIM-1. It has been reported that the formation of hydrogen bonds can make peaks shift to lower wavenumbers (cm^{-1}) with a decrease in peak intensity [44]. However, herein, no changes were observed between the FTIR spectra of PIM-1/GO-POSS, PIM/POSS and neat PIM-1 membranes, possibly due to the low concentration of fillers in the polymer matrix. It is worth noting that the N-H peak at 1463 cm^{-1} observed for POSS (Figure S9) is also observed in the GO-POSS samples. Nevertheless, for the MMMs the CH_3/CH_2 stretching at 1440 cm^{-1} overlaps with the N-H peak and no information can be inferred from it.

XRD spectra of the neat PIM-1 and the 72PGP MMMs are shown in Fig. 2a. The two main peaks of PIM-1 at 13.7° and 18.41° correspond to the micropores within the polymer structure created by the ladder-type backbone structure of PIM-1 and the chain-to-chain distance of space-packed polymer matrix, respectively [45,46]. For the MMMs, the two peaks at $2\theta = 21.5°$ and 23.8° correspond to POSS. By increasing the GO-POSS content the intensity of the first PIM-1 peak decreased. Moreover, the second peak of PIM-1 and the two characteristic peaks of POSS moved gradually towards lower 2θ values (the position of the second peak of PIM-1 is shown in Fig. 2a. This can be attributed to the interrupted chain packing of PIM-1 [47] and greater chain *d*-spacing of the membrane due to the presence of GO-POSS [11,48]. Moreover, the XRD spectra of selected 48PGP MMMs (Figure S14a) confirm the same behaviour as 72PGP MMMs, however, changes in the peak locations are smaller. XRD spectra of all PIM/POSS (PP) MMMs are displayed in Figure S14b, and no shifts are observed.

Neat PIM-1 and MMMs exhibit similar thermal stability according to the TGA results (Fig. 2b). The weight loss up to 460 °C corresponds to the removal of adsorbed moisture and volatile organic molecules [49]. The significant weight loss from 460 to 800 °C is due to polymer chain degradation and mostly ether linkage removal [19].

The cross-sectional SEM images of the neat PIM-1 and one of the MMMs (72PGP0.25) as an example are shown in Fig. 2 c&d. In certain areas of both membranes, wrinkles and polymer veins are visible, which are related to the cleanness of the fracturing method as described in section 2.5.2. The presence of the filler can increase the chance of these wrinkles appearing, with more appearing as the additive concentration goes up due to the interaction of polymer and additive [50,51]. A higher magnification SEM image of 72PGP0.25 is shown in Fig. 2d. The SEM images show no visible agglomeration of GO-POSS. The surface and cross-sectional SEM images of the other MMMs are shown in Figure S15. In some cases, the rapid evaporation of the low boiling point solvent (chloroform) resulted in small pinholes on the surface. However, the depth of the pinholes is usually less than 100 nm and they do not affect the performance of the membranes [52].

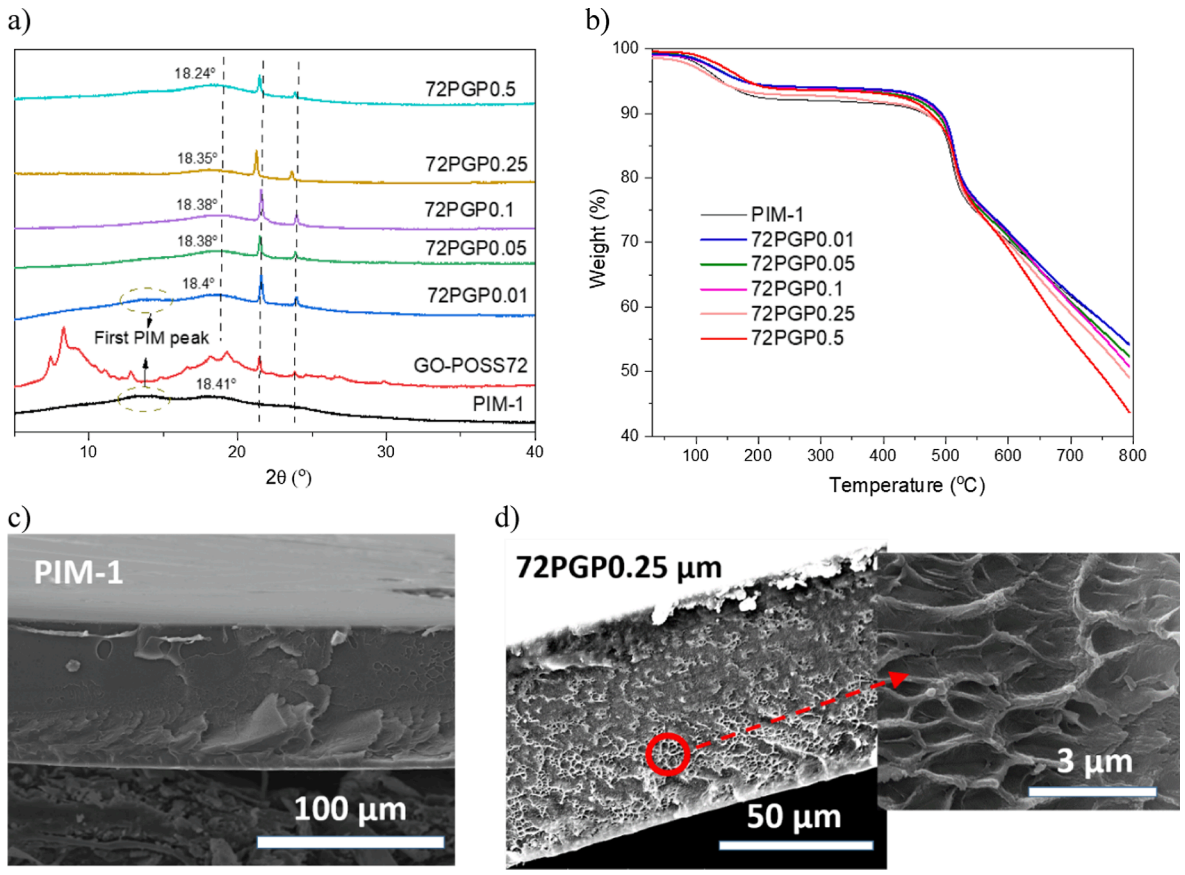

Fig. 2. Characterization of the neat PIM-1 and selected MMMs: XRD spectra (a) and TGA curves (b) of neat PIM-1 and 72PGP membranes (the dashed lines are a guideline to show the movement of the first peak of PIM-1 and POSS peaks in XRD), cross-sectional SEM image of a PIM-1 membrane (c) and 72PGP0.25 (higher magnification SEM image is shown inset) (d).

3.4. Gas separation performance

3.4.1. Fresh membranes

Single-gas permeability tests were conducted at a transmembrane pressure of 1 bar at 25 °C using gases with different kinetic diameters including H_2 (2.89 Å), CO_2 (3.3 Å), N_2 (3.64 Å), and CH_4 (3.8 Å). The gas permeability vs kinetic diameter for PIM-1 and selected PIM-1-based membranes containing GO-POSS fillers (loadings of 0.05 and 0.25 wt % of GO-POSS48 and GO-POSS72) is plotted in a graph in Figure S16. Permeability values for all tested membranes do not follow the same trend as with size: $P_{CO_2} > P_{H_2} > P_{CH_4} > P_{N_2}$, which can be related to higher solubilities for CO_2 and CH_4 as compared to H_2 and N_2, respectively, as reported elsewhere [53,54]. PIM-1 has polar groups (cyano and ether groups) in its structure that can encourage the sorption of gases such as CO_2 [53]. The PIM-1 membrane containing 0.05 wt% of GO-POSS72 deserves special attention, as it shows a more pronounced increase in CO_2 and CH_4 permeabilities as compared to all the other membranes. Solution-diffusion is the widely-accepted gas transport mechanism in PIM-1 membranes, and thus single gas measurements were performed on a constant volume/pressure increase instrument to calculate the solubility (S) and diffusivity (D) terms of the membranes (values shown in Table 1). It is observed that membrane 72PGP0.05 has ~ 4 times larger D than plain PIM-1, and reduced S (~half of the one for PIM-1). Therefore, the increase in permeability is due to a much faster diffusion of CO_2 through the MMM. It is worth noting that the GO-POSS flakes consist of non-porous GO flakes and porous POSS and the distance between two adjacent silicon atoms in POSS (4.4 Å) is bigger than the kinetic diameters of all the tested gases [48,55]. Therefore, the GO-POSS at such optimum loading must be creating additional free volume in the PIM-1 polymer matrix and/or creating additional faster permeation

Table 1
Gas permeability (P), diffusion (D) and solubility (S) coefficients and selectivity obtained with the time-lag setup for fresh membranes.

Membrane	P (Barrer)		$D \times 10^7$ ($cm^2\ s^{-1}$)		$S \times 10^3$ (cm^3 (STP) $cm^{-3}.cmHg^{-1}$)		CO_2/CH_4 ideal selectivity
	CO_2	CH_4	CO_2	CH_4	CO_2	CH_4	
PIM-1	6688	394	10.90	6.210	613.5	63.52	17.0
48PGP0.01	7321	444	41.14	7.576	178.0	58.62	16.5
48PGP0.05	8753	514	42.76	31.78	204.7	16.18	17.0
48PGP0.25	5168	637	13.55	2.908	381.5	219.1	8.1
72PGP0.01	8378	525	48.48	24.77	172.8	21.2	15.9
72PGP0.05	13,944	987	39.67	6.375	351.5	154.9	14.1
72PGP0.25	5347	325	25.13	6.992	212.8	46.44	16.4
PP0.05	11,029	648	39.36	16.82	280.3	38.52	17
PP5	5895	398	12.99	6.630	453.8	60.12	14.8

paths through the POSS NPs, while reducing available sorption sites for CO_2 in the PIM-1.

The membranes were tested for CO_2/CH_4 (50:50 v:v) separation one day after preparation and the results are plotted in a bar-like graph in Fig. 3a. The neat PIM-1 membrane showed average CO_2 and CH_4 permeabilities of 7195 ± 907 Barrer and 590 ± 93 Barrer, respectively with a CO_2/CH_4 selectivity of 12.3 ± 1.2. A wide range of permeabilities (4000–7000 [16,56]) and CO_2/CH_4 selectivity (10–20 [18]) have been reported in literature for PIM-1 due to varying polymer structures and experimental conditions. The PIM-1 synthesis can give rise to different chain structures and molecular weights, [34,57] and gas separation tests can incur a certain degree of error due to inaccurate thickness measurements, and pressure, temperature and feed composition-dependence behaviour of the membranes, which are rarely the same in literature. To determine the GO-POSS arrangement in the polymer matrix, the filler shape factor (*n* parameter in equation (10)) was optimized to obtain the best fit between predicted CO_2 permeability and experimental data (Figure S17). *n* value was found to be ~ 0.99 which means most GO-POSS nanosheets were arranged horizontally [7].

The gas separation performance of the membranes was also studied using single gases of CO_2 and N_2 at a transmembrane pressure of 1 bar, and a temperature of 25 °C. The results are presented in Fig. 3b. The neat PIM-1 membrane showed average CO_2 and N_2 permeabilities of 7323 ± 784 Barrer and 387 ± 22 Barrer, respectively with CO_2/N_2 selectivity of 18.9 ± 1.1 which is in the range of CO_2/N_2 selectivity that has been reported in the literature (16–25) [16,53]. CO_2 permeability of the MMMs indicated the same trend as CO_2/CH_4 separation. However, for CO_2/N_2 separation, all the PGP membranes showed slightly higher selectivity in comparison with the neat PIM-1 membrane, but the selectivities are in the range of error. The permeability and selectivity of all prepared membranes are presented in Table S2 of the supporting information. It should be noted that 72PGP0.75 was prepared but it was fragile and could not be tested.

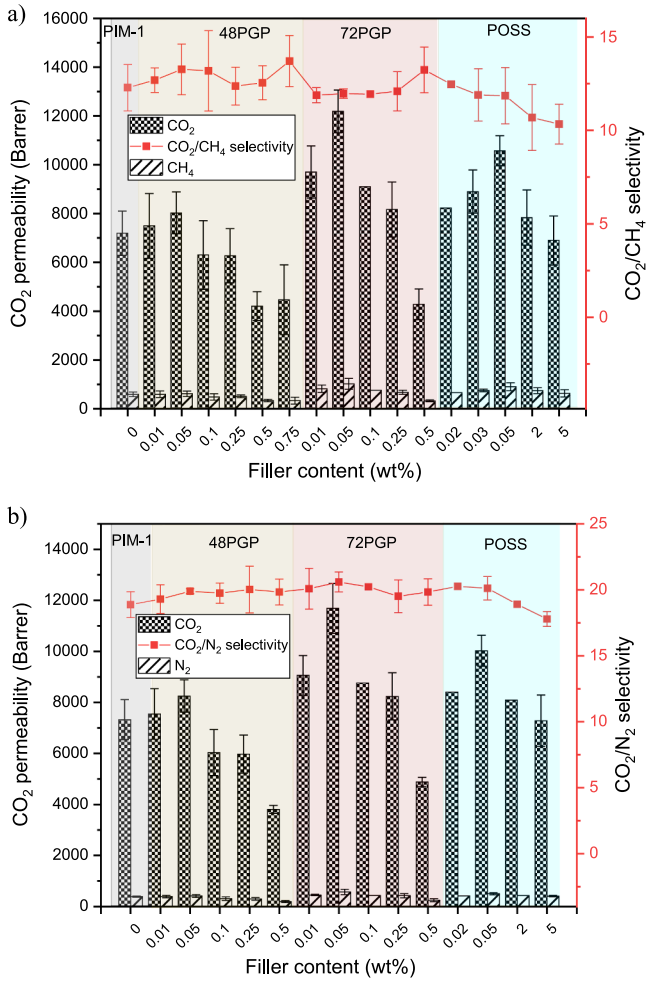

Fig. 3. Effect of GO-POSS48, GO-POSS72 and POSS on the gas separation performance of the MMMs for CO_2/CH_4 (50:50 v:v) (a) and CO_2/N_2 (single gases) (b). 3–5 samples of each kind were tested and average values and standard deviations are reported.

According to Fig. 3a, by increasing the GO-POSS48 and GO-POSS72 loadings up to 0.05 wt%, the CO_2 permeability increased to 8025 ± 857 Barrer (CO_2/CH_4 selectivity: 13.3 ± 1.3) and 12185 ± 1547 Barrer (CO_2/CH_4 selectivity: 12.0 ± 0.2), respectively. The gas transport through the membranes can happen by three paths: 1) PIM-1 free volume, 2) interlayer space of GO-POSS, 3) interface between filler and PIM-1 polymer chains. Further increases in filler content decreased the CO_2 permeability, possibly due to the rigidification of the polymer chains, as well as the increased tortuosity resulting from the high aspect ratio of GO laminates (deposited horizontally inside the polymer matrix as confirmed with the Maxwell equation). In addition, higher concentrations of GO-POSS may cause pore blockage, decreases the effective porosity as well as decreasing the membrane's gas solubility due to the relative reduction in polymer content (Table 1) [11,58,59]. It has been reported that nonporous fillers can restrict the diffusion of larger molecules but they may provide near frictionless channels for smaller molecules and increase the selectivity of the membrane [60]. However, different behaviours have been reported by introducing nonporous fillers in the PIM-1 polymer structure. Luque-Alled et al. [19] prepared (PIM-1)-functionalized GO derivatives/PIM-1 MMMs, and all the membranes (regardless of the filler concentrations) showed lower permeability and higher CO_2/CH_4 selectivity in comparison with neat PIM-1 membrane, however, on adding GO-OA and GO-ODA both permeability and selectivity decreased [18]. In this study, all the PGP MMMs have almost the same or higher selectivity than neat PIM-1. This can be attributed to the good compatibility of filler and polymer chains that can minimize interfacial voids. Moreover, the good solubility of GO-POSS in chloroform can facilitate adequate distribution of filler in the MMMs.

The diffusion (*D*) and solubility (*S*) values of the fresh neat PIM-1 and selected MMMs for CO_2 and CH_4 are shown in Table 1. It should be noted that in the time-lag instrument, the membranes were first tested for CO_2 for 5 days and then for CH_4. This may be the reason for the higher single-gas selectivity (due to aging) compared to the gas mixture (Fig. 3a). The highest permeability and diffusion coefficient occurred at the filler loading of 0.05 wt% for both 48PGP and 72PGP MMMs (same as the CO_2/CH_4 gas mixture separation). Also, the *D* values of all MMMs are greater than neat PIM-1 with a maximum at 0.05 wt% of the filler. This confirms the higher FFV of the MMMs at low filler concentrations (caused by the disruption in the packing of the polymer chains) as well as PIM-1 pores blockage at higher loadings (0.25 wt% for PGP and 5 wt % for PP), which counteracts the first effect and thereby decreasing the gas diffusion coefficient. The permeability enhancement at low filler loadings can be due to the higher *D* values of the MMMs (due to chain packing disruption) [11,61] and also the larger *d*-spacing of GO-POSS compared to GO (meaning gas molecules can diffuse between adjacent GO-POSS sheets). It should be noted that the *d*-spacing of GO-POSS72 is larger than GO-POSS48 as confirmed by XRD results (section 3.2).

According to Table 1, there is no specific relationship between the filler loadings and solubility coefficients; however, *S* values for all MMMs are smaller than that for neat PIM-1. This indicates that some of the sorption sites of PIM-1 are not accessible due to the presence of the filler [7].

PIM/POSS (PP) MMMs (without GO) were fabricated as described in the experimental section. The POSS loadings in the PP membranes were 0.02, 0.03, 0.05, 2 and 5 wt%. The range was selected based on the estimated content of just POSS in the best performing PGP membranes. The membrane with the highest permeability among the prepared PGP

membranes has a loading of GO-POSS72 of 0.05 wt% (membrane 72PGP0.05), and the POSS mass fraction of filler GO-POSS72 is 0.46 based on TGA results (section 3.2). Thus, the concentration of only POSS in this membrane is 0.02 wt% ($0.05 \times 0.46 = 0.02$). Much higher concentrations up to 5 wt% were prepared to study the possible interaction of amine groups in POSS and CO_2 gas molecules, as it has been reported that amine groups can react with CO_2 and improve the separation performance [62].

The highest permeability was obtained at a loading of 0.05 wt% POSS (10575 ± 609 Barrer), which represents a 47% increase in comparison with that of the neat PIM-1 membrane (Fig. 3a). The higher permeability of 72PGP0.05 compared to PP0.02 (same POSS content for both), may be explained by the higher FFV of the PGP membranes as confirmed by XRD results. Even though the kinetic diameters of the tested gases are smaller than the pore size of POSS (4.4 Å), their permeability decreases as POSS concentration increases (following a similar trend to that for GO-POSS), with a final permeability that was slightly lower than that of the pure PIM-1 membrane. There are two possible explanations for this. First, rigidification of PIM-1 polymer chain at high POSS loadings [63] and second, partial blockage of POSS pores by polymer chain [64]. In addition, different types of POSS have been reported in PIM-1 [11] and poly[1-(trimethylsilyl)-1-propyne] (PTMSP) [65] membranes. These studies have reported that despite their porosity, POSS nanoparticles act as nonporous fillers, increasing tortuosity and extent of polymer pore blockage at high loadings and thus reducing membrane permeability. This is evidenced by the much lower value of CO_2 diffusivity for PP5 (Table 1) as compared to the values of PP0.05 and the rest of the tested MMMs. Figure S16j shows an inset with a high magnification cross-sectional SEM image of a PP5 membrane that suggests good dispersion and no agglomeration of POSS nanoparticles into PIM-1.

Moreover, the CO_2/CH_4 selectivity of the PP membranes slightly decreased by increasing POSS concentration from 0.05 to 5 wt% (11.8 vs 10.4). The addition of high loadings of up to 5 wt% of POSS (membrane PP5) does not lead to higher solubility diffusivities and thus, low interaction (or no interaction) of available amine groups in POSS with CO_2 can be expected.

Yong et al. [11] fabricated PIM-1/DiSilanolIsobutyl POSS MMMs. The highest permeability was achieved at the lowest POSS loading (0.5 wt%), which showed a 35% enhancement in CO_2 permeability in comparison with a neat PIM-1 membrane. This was attributed to the higher FFV of MMMs as well as the reaction of Si-OH group on POSS with CO_2. However, at higher POSS loadings (>2 wt%) the pores were blocked and the *d*-spacing of the polymer chains decreased, which induced an increase in CO_2/CH_4 selectivity and a decline in CO_2 permeability. Konnertz et al. [66] indicated that the highest permeability of PIM-1 MMMs was at the lowest loading of 1 wt% PhenethylPOSS. However, the permeability of the MMMs at lower filler loadings (less than 1 wt%) was not investigated. The permeability enhancement at low filler loading was assigned to the disrupted polymer chains.

The effect of a more intense thermal treatment of the GO-POSS nanohybrids (reduced sample rGO-POSS72 obtained at 120 °C for 8 h) on the gas separation performance of the MMMs was studied and results are plotted in a graph in Figure S18. Membranes containing rGO-POSS at a loading of 0.05 wt% also showed very similar CO_2/CH_4 selectivity values and higher CO_2 permeability than purely PIM-1 membranes. However, the permeability increase was not as pronounced as that of MMMs with non-reduced GO-POSS72 nanohybrids. The XRD spectra of both fillers (Fig. 1c) indicate a slightly more disordered material for the reduced sample, but there are no significant differences in their structures which can account for the differences in permeability. Therefore, it is hypothesized that the thermal treatment at 120 °C can lead to the disappearance of remaining un-reacted oxygen-containing functional groups still present after the functionalization reaction (as reported elsewhere [28]), that can in fact affect the gas separation performance of the PIM-1 membranes. Yet, the mechanism for this is unclear and further research should be conducted.

The effect of feed (CO_2/CH_4) composition at the constant transmembrane pressure of 1 bar on the performance of selected membranes was studied and is shown in Figure S19. By increasing the volume fraction of CO_2 in the feed, the more condensable penetrant species (CO_2) tend to occupy the Langmuir sites (microvoids in the polymer matrix) and reduces the permeability of CH_4. Therefore, CO_2/CH_4 selectivity for a gas mixture is slightly higher than the ideal selectivity (single gases) [67]. In addition to competitive sorption on Langmuir sites, plasticization (which occurs at high CO_2 partial pressures) can also contribute to a change in selectivity. To study the effect of pressure, neat PIM-1, 72PGP0.25, and 48PGP0.25 membranes were tested at a total feed pressure in the range of 20–130 psi (1.4–9 bar), which is the limit in our setup, using a CO_2/CH_4 (50:50 v:v) mixture as the feed (Figure S20). On increasing the pressure, the CO_2 permeability decreased and no sign of plasticization was observed up to 9 bar. This is in agreement with literature that shows no plasticization of PIM-1-based membranes up to 440 psi (30 bar) [11]. Lower permeability at higher pressures may be due to membrane compression (pore size reduction). It is worth noting that the permeability reduction is more significant for the neat PIM-1 membrane as compared to that of the MMMs, which can be due restriction in polymer chain mobility when the filler is added. The CO_2/CH_4 selectivity, meanwhile, stays almost constant with increasing pressure.

3.4.2. Aged membranes

The aging performance of PGP and PP MMMs for CO_2/N_2 and CO_2/CH_4 separation was studied and the results are shown in Table S2 of the supporting information. For each membrane variant, 3 to 5 samples were prepared. For some of the aged membranes only one sample survived after 160 days, probably due to loading/unloading into the gas separation cell several times, and therefore standard deviations are not provided for those samples.

Graphs with CO_2 permeability and CO_2/CH_4 selectivity versus aging time for the neat PIM-1 membrane and selected MMMs are displayed in Fig. 4 a&b. Values for the CO_2 permeability drop (calculated with equation (4)) and the relative CO_2 permeability (calculated with equation (5)) are shown in Fig. 4 c&d, respectively. For each type of filler (GO-POSS48, GO-POSS72 and POSS), the results of two membranes that have the highest initial permeability (48PGP0.05, 72PGP0.05 and PP0.05) and the best aging behaviour (48PGP0.75, 72PGP0.25 and PP2) are shown. In addition, the results of 48PGP0.25 are indicated for a fair comparison with 72PGP0.25.

Polymer chain relaxation over time decreased the free volume of the membrane, and this affected the diffusion of molecules with a larger kinetic diameter more than the smaller molecules, [68] which translated into the general trend of increased CO_2/CH_4 selectivity upon aging that was observed (Fig. 4b). It is worth noting that there were random decreases in selectivity for some of these samples in between the testing period, that could be due to defects from loading/unloading of the membrane coupons several times into the gas separation cell. For each membrane, 3 to 5 coupons were prepared and tested, for instance, 5 fresh samples were tested for 48PGP0.25, but only two samples survived after 125 days. It is therefore possible that small defects formed in some of the aged membranes during handling, specially in the epoxy resin/membrane region (thus increasing permeability), that became more evident in the next aging test (due to further membrane handling) and thus that coupon was disregarded for that last and subsequent data points. According to Fig. 4c, the permeability drop was more pronounced during the first 21 days, followed by a gradual decrease, which is in agreement with the literature [68]. After 160 days of aging, the membranes containing 0.05 wt% of fillers (48PGP0.05, 72PGP0.05 and PP0.05) showed a higher CO_2 permeability drop than that of neat PIM-1. However, the permeability of all MMMs was higher than that of purely polymeric PIM-1 membranes. In addition, the CO_2 permeability reduction of the aged PP MMMs was higher than that of PGP membranes (at

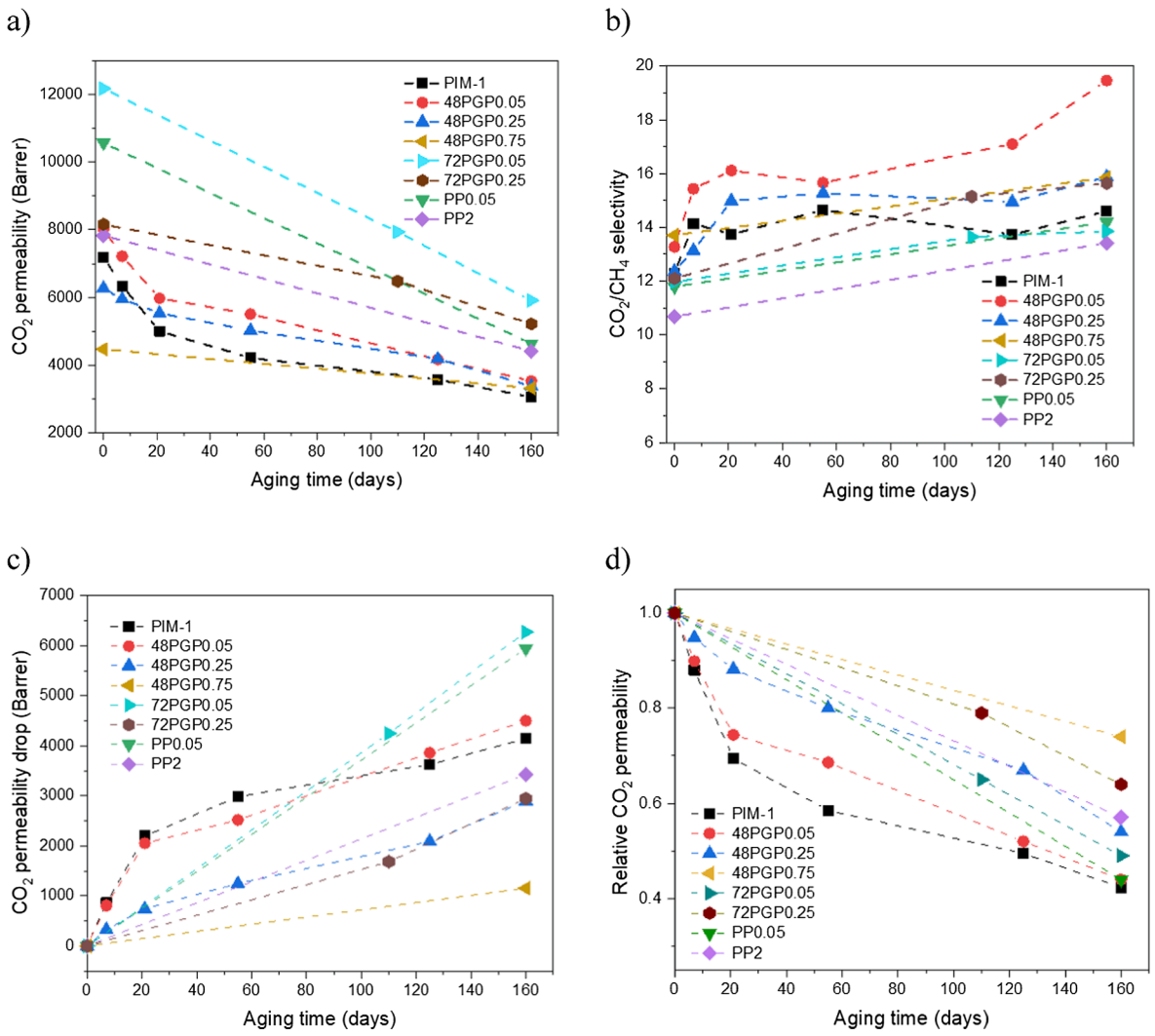

Fig. 4. Evolution up to 160 days of CO_2 permeability (a), CO_2/CH_4 selectivity (b), CO_2 permeability drop (c), relative CO_2 permeability (d) of PIM-1 and selected MMMs.

the same POSS concentrations), which confirms the positive effect GO flakes has on physical aging inhibition.

Both the initial CO_2 permeability and the permeability drop decreased by increasing the concentration of the filler above 0.0.5 wt%. 48PGP0.75 exhibited the lowest permeability drop (1153 Barrer) and the highest relative CO_2 permeability (0.74), which was attributed to the higher rigidification effects (interactions of the filler with the polymer chain) at higher filler loading [22]. It should be noted that from the operational point of view a membrane with higher stability is preferred over a membrane with higher initial permeability but higher permeability drop. The stability is vital for thin film composite (TFC) PIM-1 membranes because of the more pronounced effect of physical aging; for instance, a 200 nm thick PIM-1 membrane can lose 95% of its initial CO_2 permeability in less than three months after preparation [69].

The aging behaviour of PIM-1 membranes can be affected by different parameters including the PIM-1 polymer chain structure, [7,70] membrane thickness, [71] post-treatments (alcohol (MeOH and ethanol) treatment), [68] and membrane storage conditions. Foster et al. [34,70] studied the effect of the presence of branched PIM-1 chains on the performance and aging behaviour of neat PIM-1 membranes. They found that the PIM-1 membrane with the branched-chain experienced slower physical aging compared to the PIM-1 membrane with a linear polymeric structure. In our study, the presence of the branched PIM-1 structure is confirmed by NMR and MALDI-TOF characterizations. This can be the reason for the higher relative CO_2 permeability of the aged neat PIM-1 membrane in this investigation compared to our previous study (Table 2) [18]. Moreover, the alcohol-treated membranes demonstrate a slight increase in thickness accompanied by size shrinkage. This can be caused by stress-relaxation of the membranes and induces an enhancement in preventing physical aging [7]. In addition, thermal treatment (membrane drying after alcohol treatment) aids the polymer chain relaxation and brings about a lower permeability drop over time [68].

Different nanosheets and POSS have been used as a filler in the literature to suppress the physical aging of the PIM-1 membrane. The initial and relative CO_2 permeability of these membranes after a specific aging time are compared in Table 2. It should be noted that the highest loading of the filler does not always increase the inhibition of physical aging due to the filler agglomeration above the optimum concentration. Alberto et al. [18] prepared PIM-1/graphene-like materials MMMs at the concentration range of 0.01–0.25 wt% and the best physical aging impediment was achieved at a low loading of the filler (0.05 wt%). Ameen et al. [7] prepared PIM/boron nitride nanosheets (BNNs) at two different BNNs concentrations of 0.5 wt% and 0.8 wt%. The best membrane performance in terms of aging was achieved at 0.5 wt% BNNs.

The CO_2/CH_4 and CO_2/N_2 separation performances of the selected prepared membranes have been compared with some of the MMMs

Table 2
Comparison of data obtained for PIM-1 MMMs in this work with data from the literature.

Membrane (wt% of filler)	Initial CO_2 permeability (Barrer)	Aging days	Relative CO_2 permeability	Reference
Neat PIM-1	7194	160	0.42	This study
48PGP (0.75)	4462	160	0.74	This study
72PGP (0.05)	12,185	160	0.49	This study
Neat PIM-1	6190	150	0.53	[19]
PIM/APTS-GO (0.1)	5785	120	0.61	[19]
PIM/Boron nitride (0.5)	5940	102	0.9	[7]
Neat PIM-1	6400	155	0.31	[18]
PIM/ODA-rGO (0.05)	4700	155	0.51	[18]
PIM/octylamine (OA)-rGO (0.05)	5700	155	0.62	[18]
PIM/PEG-POSS (10)	1309	30	0.8	[47]
PIM/amino POSS (5)	3811	90	0.73	[16]
PIM/low cross-link density (LCD) network-PIM-1	12,500	120	0.71	[56]
PIM/few layer graphene	9840	240	0.78	[17]

reported in previous studies [7,18,19] using the upper-bound plot. The upper limit represents the trade-off of permeability and selectivity of polymeric membranes. According to Fig. 5a, the performances of fresh MMMs (PGP0.05 and PP0.05) and the neat PIM-1 membrane laid above the 2008 upper bound and moved towards lower permeability and higher selectivity over time. However, after 160 days of aging, the PIM-1 membrane data point was lower than the 2008 upper bound. PIM-1/LCD network PIM-1 [56] (pink right-pointing triangle in Fig. 5a) exhibited almost the same initial performance as PGP0.05 however, its aging behaviour was better and the membrane showed a lower permeability drop. The data point of PIM-1/ODA-rGO (0.05 wt%) [18] (purple diamond in Fig. 5a) is near to 2019 upper bound but it lost half of its initial CO_2 permeability after 155 days.

For CO_2/N_2 separation (Fig. 5b), data points of all membranes surpass the 2008 Robeson upper-bound and 72PGP0.05 and PP0.05 performances are near the 2019 upper-bound. After 160 days, the data point of PIM-1 drops below the Robeson upper bound and those of PP0.05 and 48PGP0.05 lie on the upper bound. However, for 72PGP0.05, the data point stays above the upper bound. The increment in CO_2/N_2 selectivity of the aged membranes does not occur at the same proportion as CO_2/CH_4. For instance, the CO_2/CH_4 selectivity increased from 13.3 for 48PGP0.05 to 19.4 after 160 days of aging. However, at the same time, CO_2/N_2 selectivity only increased from 19.9 to 20.8. It seems that a reduction in the free volume of the polymer matrix over time affects condensable gases (CO_2 and CH_4) more than non-condensable gas (N_2).

The H_2/N_2 separation performances of fresh membranes are shown in Figure S21. The data points of the membranes lay below the 2008 Robeson upper bound except for 72PGP0.05.

4. Conclusions

In conclusion, the gas separation performance of PIM-1 membranes has been enhanced in terms of permeability (without any sacrifice in the CO_2/CH_4 and CO_2/N_2 selectivity) and aging resistance by incorporating POSS-functionalized GO as a filler.

Longer functionalization reaction time of GO with POSS led to

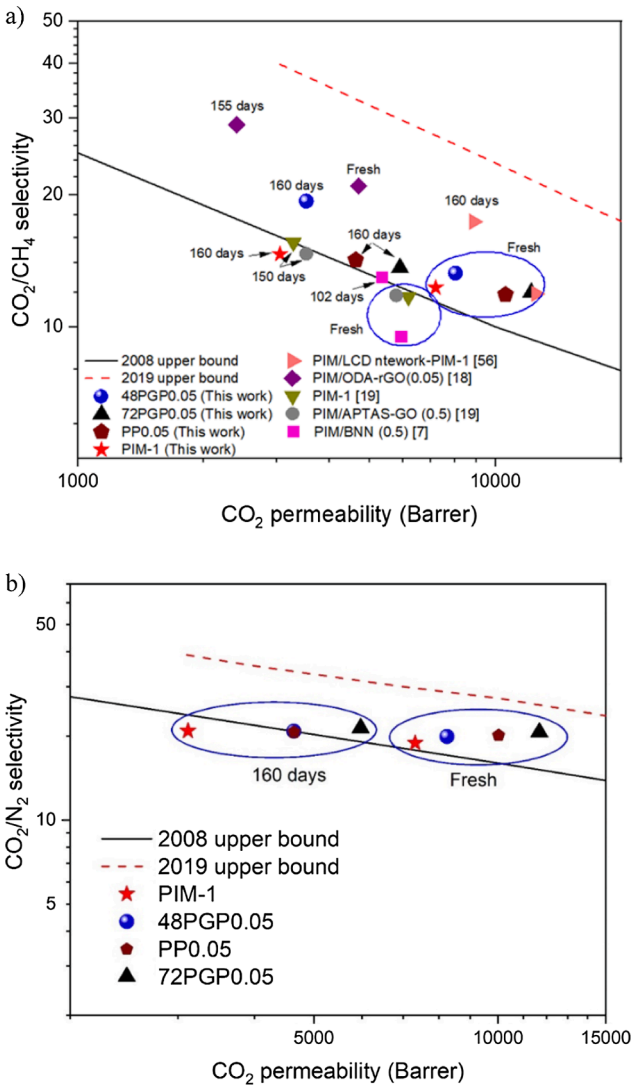

Fig. 5. Double logarithmic plot of CO_2/CH_4 (a) and CO_2/N_2 (b) selectivity versus CO_2 permeability for neat PIM-1 and MMMs containing 0.05 wt% of GO-POSS48 (48PGP0.05), GO-POSS72 (72PGP0.05), and POSS (PP0.05). Also, 2008 Robeson upper bound [72] and 2019 Jansen and McKeown upper bound [73] are plotted. For CO_2/CH_4 separation, the performance of the membranes compared with some of the other membranes reported in literature [7,18,19,56].

membranes with higher permeability due to the higher interlayer spacing of the GO-POSS72 sample. The optimum loading of the filler with respect to the polymer was 0.05 wt%, which increased the permeability by 69%, from 7195 Barrer for neat PIM-1 membrane to ~ 12000 Barrer, with a CO_2/CH_4 selectivity of 12 and CO_2/N_2 selectivity of 20.6.

The effect of the physical aging on the gas permeability of the fabricated membranes was studied over a 5-month period; higher filler loadings led to lower initial permeability but also to smaller CO_2 permeability drop over time. Also, the MMMs prepared with GO-POSS presented higher resistance to aging compared to POSS alone, which was attributed to the presence of high aspect ratio GO flakes that induced rigidification of PIM-1 polymer chains and inhibited the migration of PIM-1 polymer chains over time. All MMMs outperform the neat PIM-1 membrane in terms of permeability 160 days after preparation. Furthermore, the initial performance of the membranes was better preserved for the MMM containing the GO-POSS flakes reacted for shorter times (48 h) at low filler loadings of 0.75 wt% (48PGP0.75). This

is essential for PIM-1 to reach the commercialization stage for gas separation applications.

Credit authorship contribution statement

Sajjad Mohsenpour: Conceptualization, Investigation, Methodology, Formal analysis, Visualization, Writing – original draft. **Ahmed W. Ameen:** Methodology. **Sebastian Leaper:** Investigation, Methodology. **Clara Skuse:** Methodology. **Faiz Almansour:** Methodology. **Peter M. Budd:** Conceptualization, Supervision, Writing – review & editing. **Patricia Gorgojo:** Conceptualization, Supervision, Project administration, Funding acquisition, Writing – review & editing.

Declaration of Competing Interest

The authors declare that they have no known competing financial interests or personal relationships that could have appeared to influence the work reported in this paper.

Acknowledgments

S. Mohsenpour thanks the University of Manchester for funding his Ph.D. studies. P. Gorgojo acknowledges the Spanish Ministry of Economy and Competitiveness and the European Social Fund through the Ramon y Cajal programme (RYC2019-027060-I/AEI/10.13039/501100011033).

Appendix A. Supplementary material

Supplementary data to this article can be found online at https://doi.org/10.1016/j.seppur.2022.121447.

References

[1] A. Haines, R.S. Kovats, D. Campbell-Lendrum, C. Corvalan, Climate change and human health: impacts, vulnerability and public health, Public health 120 (7) (2006) 585–596.
[2] J. Tollefson, IPCC says limiting global warming to 1.5 C will require drastic action, Nature 562 (7726) (2018) 172–173.
[3] S. Shah, M. Shah, A. Shah, M. Shah, Evolution in the membrane-based materials and comprehensive review on carbon capture and storage in industries, Emergent Mater. 3 (1) (2020) 33–44.
[4] L. Deng, M.-B. Hägg, Techno-economic evaluation of biogas upgrading process using CO2 facilitated transport membrane, Int. J. Greenhouse Gas Control 4 (4) (2010) 638–646.
[5] Y. Zhang, J. Sunarso, S. Liu, R. Wang, Current status and development of membranes for CO2/CH4 separation: A review, Int. J. Greenhouse Gas Control 12 (2013) 84–107.
[6] J. Contreras-Martínez, S. Mohsenpour, A.W. Ameen, P.M. Budd, C. García-Payo, M. Khayet, P. Gorgojo, High-Flux Thin Film Composite PIM-1 Membranes for Butanol Recovery: Experimental Study and Process Simulations, ACS Appl. Mater. Interfaces 13 (36) (2021) 42635–42649.
[7] A.W. Ameen, J. Ji, M. Tamaddondar, S. Moshenpour, A.B. Foster, X. Fan, P. M. Budd, D. Mattia, P. Gorgojo, 2D boron nitride nanosheets in PIM-1 membranes for CO2/CH4 separation, J. Membr. Sci. 636 (2021) 119527.
[8] M.R. Khdhayyer, E. Esposito, A. Fuoco, M. Monteleone, L. Giorno, J.C. Jansen, M. P. Attfield, P.M. Budd, Mixed matrix membranes based on UiO-66 MOFs in the polymer of intrinsic microporosity PIM-1, Sep. Purif. Technol. 173 (2017) 304–313.
[9] M. Khdhayyer, A.F. Bushell, P.M. Budd, M.P. Attfield, D. Jiang, A.D. Burrows, E. Esposito, P. Bernardo, M. Monteleone, A. Fuoco, G. Clarizia, F. Bazzarelli, A. Gordano, J.C. Jansen, Mixed matrix membranes based on MIL-101 metal–organic frameworks in polymer of intrinsic microporosity PIM-1, Sep. Purif. Technol. 212 (2019) 545–554.
[10] S. He, et al., Recent progress in PIM-1 based membranes for sustainable CO2 separations: Polymer structure manipulation and mixed matrix membrane design, Sep. Purif. Technol. 284 (2022), 120277.
[11] W.F. Yong, K.H.A. Kwek, K.-S. Liao, T.-S. Chung, Suppression of aging and plasticization in highly permeable polymers, Polymer 77 (2015) 377–386.
[12] Z.-X. Low, P.M. Budd, N.B. McKeown, D.A. Patterson, Gas permeation properties, physical aging, and its mitigation in high free volume glassy polymers, Chem. Rev. 118 (12) (2018) 5871–5911.
[13] G. Dong, H. Li, V. Chen, Challenges and opportunities for mixed-matrix membranes for gas separation, J. Mater. Chem. A 1 (15) (2013) 4610–4630.
[14] C.H. Lau, P.T. Nguyen, M.R. Hill, A.W. Thornton, K. Konstas, C.M. Doherty, R. J. Mulder, L. Bourgeois, A.C.Y. Liu, D.J. Sprouster, J.P. Sullivan, T.J. Bastow, A. J. Hill, D.L. Gin, R.D. Noble, Ending aging in super glassy polymer membranes, Angew. Chem. Int. Ed. 53 (21) (2014) 5322–5326.
[15] M.M. Khan, V. Filiz, G. Bengtson, S. Shishatskiy, M.M. Rahman, J. Lillepaerg, V. Abetz, Enhanced gas permeability by fabricating mixed matrix membranes of functionalized multiwalled carbon nanotubes and polymers of intrinsic microporosity (PIM), J. Membr. Sci. 436 (2013) 109–120.
[16] Y. Kinoshita, K. Wakimoto, A.H. Gibbons, A.P. Isfahani, H. Kusuda, E. Sivaniah, B. Ghalei, Enhanced PIM-1 membrane gas separation selectivity through efficient dispersion of functionalized POSS fillers, J. Membr. Sci. 539 (2017) 178–186.
[17] K. Althumayri, et al., The influence of few-layer graphene on the gas permeability of the high-free-volume polymer PIM-1, Philosophical Transactions of the Royal Society A: Mathematical, Physical and Engineering Sciences 374 (2060) (2016) 20150031.
[18] M. Alberto, R. Bhavsar, J.M. Luque-Alled, A. Vijayaraghavan, P.M. Budd, P. Gorgojo, Impeded physical aging in PIM-1 membranes containing graphene-like fillers, J. Membr. Sci. 563 (2018) 513–520.
[19] J.M. Luque-Alled, et al., Gas separation performance of MMMs containing (PIM-1)-functionalized GO derivatives, J. Membr. Sci. 623 (2021), 118902.
[20] W. Chen, et al., Metal-organic framework MOF-801/PIM-1 mixed-matrix membranes for enhanced CO2/N2 separation performance, Sep. Purif. Technol. 250 (2020), 117198.
[21] M. Jia, Y.i. Feng, J. Qiu, X.-F. Zhang, J. Yao, Amine-functionalized MOFs@ GO as filler in mixed matrix membrane for selective CO2 separation, Sep. Purif. Technol. 213 (2019) 63–69.
[22] J.M. Luque-Alled, M. Tamaddondar, A.B. Foster, P.M. Budd, P. Gorgojo, PIM-1/Holey Graphene Oxide Mixed Matrix Membranes for Gas Separation: Unveiling the Role of Holes, ACS Appl. Mater. Interfaces 13 (46) (2021) 55517–55533.
[23] W. Zhang, A.H. Müller, Architecture, self-assembly and properties of well-defined hybrid polymers based on polyhedral oligomeric silsequioxane (POSS), Prog. Polym. Sci. 38 (8) (2013) 1121–1162.
[24] K. Tanaka, Y. Chujo, Advanced functional materials based on polyhedral oligomeric silsesquioxane (POSS), J. Mater. Chem. 22 (5) (2012) 1733–1746.
[25] Y. Xue, Y. Liu, F. Lu, J. Qu, H. Chen, L. Dai, Functionalization of graphene oxide with polyhedral oligomeric silsesquioxane (POSS) for multifunctional applications, J. Phys. Chem. Lett. 3 (12) (2012) 1607–1612.
[26] T. Emmler, K. Heinrich, D. Fritsch, P.M. Budd, N. Chaukura, D. Ehlers, K. Rätzke, F. Faupel, Free volume investigation of polymers of intrinsic microporosity (PIMs): PIM-1 and PIM1 copolymers incorporating ethanoanthracene units, Macromolecules 43 (14) (2010) 6075–6084.
[27] L. Zhang, W. Fang, J. Jiang, Effects of residual solvent on membrane structure and gas permeation in a polymer of intrinsic microporosity: insight from atomistic simulation, J. Phys. Chem. C 115 (22) (2011) 11233–11239.
[28] S. Leaper, E.O. Avendaño Cáceres, J.M. Luque-Alled, S.H. Cartmell, P. Gorgojo, Poss-Functionalized Graphene Oxide/PVDF Electrospun Membranes for Complete Arsenic Removal Using Membrane Distillation, ACS Appl. Polym. Mater. 3 (4) (2021) 1854–1865.
[29] L. Gao, M. Alberto, P. Gorgojo, G. Szekely, P.M. Budd, High-flux PIM-1/PVDF thin film composite membranes for 1-butanol/water pervaporation, J. Membr. Sci. 529 (2017) 207–214.
[30] Cullity, B.D., *Elements of X-ray Diffraction*. 1956: Addison-Wesley Publishing.
[31] Q. Qian, P.A. Asinger, M.J. Lee, G. Han, K. Mizrahi Rodriguez, S. Lin, F. M. Benedetti, A.X. Wu, W.S. Chi, Z.P. Smith, MOF-based membranes for gas separations, Chem. Rev. 120 (16) (2020) 8161–8266.
[32] L. Yang, et al., Amino-functionalized POSS nanocage intercalated graphene oxide membranes for efficient biogas upgrading, J. Membr. Sci. 596 (2020), 117733.
[33] N. Tien-Binh, D. Rodrigue, S. Kaliaguine, In-situ cross interface linking of PIM-1 polymer and UiO-66-NH2 for outstanding gas separation and physical aging control, J. Membr. Sci. 548 (2018) 429–438.
[34] A.B. Foster, M. Tamaddondar, J.M. Luque-Alled, W.J. Harrison, Z.e. Li, P. Gorgojo, P.M. Budd, Understanding the topology of the polymer of intrinsic microporosity PIM-1: cyclics, tadpoles, and network structures and their impact on membrane performance, Macromolecules 53 (2) (2020) 569–583.
[35] O.C. Compton, D.A. Dikin, K.W. Putz, L.C. Brinson, S.T. Nguyen, Electrically conductive "alkylated" graphene paper via chemical reduction of amine-functionalized graphene oxide paper, Adv. Mater. 22 (8) (2010) 892–896.
[36] F. Zhou, H.N. Tien, Q. Dong, W.L. Xu, H. Li, S. Li, M. Yu, Ultrathin, ethylenediamine-functionalized graphene oxide membranes on hollow fibers for CO2 capture, J. Membr. Sci. 573 (2019) 184–191.
[37] Y. Lu, S. Zhang, Z. Geng, K. Zhu, M. Zhang, R. Na, G. Wang, Hybrid formation of graphene oxide–POSS and their effect on the dielectric properties of poly (aryl ether ketone) composites, New J. Chem. 41 (8) (2017) 3089–3096.
[38] X. Zhi, Y. Mao, Z. Yu, S. Wen, Y. Li, L. Zhang, T.W. Chan, L.i. Liu, γ-Aminopropyl triethoxysilane functionalized graphene oxide for composites with high dielectric constant and low dielectric loss, Compos. A Appl. Sci. Manuf. 76 (2015) 194–202.
[39] X.-Z. Tang, W. Li, Z.-Z. Yu, M.A. Rafiee, J. Rafiee, F. Yavari, N. Koratkar, Enhanced thermal stability in graphene oxide covalently functionalized with 2-amino-4, 6-didodecylamino-1, 3, 5-triazine, Carbon 49 (4) (2011) 1258–1265.
[40] W.-S. Hung, C.-H. Tsou, M. De Guzman, Q.-F. An, Y.-L. Liu, Y.-M. Zhang, C.-C. Hu, K.-R. Lee, J.-Y. Lai, Cross-linking with diamine monomers to prepare composite graphene oxide-framework membranes with varying d-spacing, Chem. Mater. 26 (9) (2014) 2983–2990.
[41] S. Park, D.A. Dikin, S.T. Nguyen, R.S. Ruoff, Graphene oxide sheets chemically cross-linked by polyallylamine, J. Phys. Chem. C 113 (36) (2009) 15801–15804.
[42] F. Zhou, H.N. Tien, W.L. Xu, J.-T. Chen, Q. Liu, E. Hicks, M. Fathizadeh, S. Li, M. Yu, Ultrathin graphene oxide-based hollow fiber membranes with brush-like CO2-philic agent for highly efficient CO2 capture, Nat. Commun. 8 (1) (2017).

[43] H. Li, Z. Song, X. Zhang, Y.i. Huang, S. Li, Y. Mao, H.J. Ploehn, Y.u. Bao, M. Yu, Ultrathin, molecular-sieving graphene oxide membranes for selective hydrogen separation, Science 342 (6154) (2013) 95–98.
[44] Y. Pu, et al., Amino-functionalized NUS-8 nanosheets as fillers in PIM-1 mixed matrix membranes for CO2 separations, J. Membr. Sci. 641 (2022), 119912.
[45] L. Hao, K.-S. Liao, T.-S. Chung, Photo-oxidative PIM-1 based mixed matrix membranes with superior gas separation performance, J. Mater. Chem. A 3 (33) (2015) 17273–17281.
[46] W.F. Yong, F.Y. Li, T.-S. Chung, Y.W. Tong, Highly permeable chemically modified PIM-1/Matrimid membranes for green hydrogen purification, J. Mater. Chem. A 1 (44) (2013) 13914.
[47] L. Yang, Z. Tian, X. Zhang, X. Wu, Y. Wu, Y. Wang, D. Peng, S. Wang, H. Wu, Z. Jiang, Enhanced CO2 selectivities by incorporating CO2-philic PEG-POSS into polymers of intrinsic microporosity membrane, J. Membr. Sci. 543 (2017) 69–78.
[48] M.L. Chua, L.u. Shao, B.T. Low, Y. Xiao, T.-S. Chung, Polyetheramine–polyhedral oligomeric silsesquioxane organic–inorganic hybrid membranes for CO2/H2 and CO2/N2 separation, J. Membr. Sci. 385-386 (2011) 40–48.
[49] B. Satilmis, P.M. Budd, Base-catalysed hydrolysis of PIM-1: amide versus carboxylate formation, RSC Adv. 4 (94) (2014) 52189–52198.
[50] Y. Cheng, X. Wang, C. Jia, Y. Wang, L. Zhai, Q. Wang, D. Zhao, Ultrathin mixed matrix membranes containing two-dimensional metal-organic framework nanosheets for efficient CO2/CH4 separation, J. Membr. Sci. 539 (2017) 213–223.
[51] Z. Hu, Z. Kang, Y. Qian, Y. Peng, X. Wang, C. Chi, D. Zhao, Mixed matrix membranes containing UiO-66 (Hf)-(OH) 2 metal–organic framework nanoparticles for efficient H2/CO2 separation, Ind. Eng. Chem. Res. 55 (29) (2016) 7933–7940.
[52] J. Li, et al., PIM-1 pore-filled thin film composite membranes for tunable organic solvent nanofiltration, J. Membr. Sci. 601 (2020), 117951.
[53] P. Budd, K. Msayib, C. Tattershall, B. Ghanem, K. Reynolds, N. Mckeown, D. Fritsch, Gas separation membranes from polymers of intrinsic microporosity, J. Membr. Sci. 251 (1-2) (2005) 263–269.
[54] P. Budd, N. Mckeown, B. Ghanem, K. Msayib, D. Fritsch, L. Starannikova, N. Belov, O. Sanfirova, Y. Yampolskii, V. Shantarovich, Gas permeation parameters and other physicochemical properties of a polymer of intrinsic microporosity: Polybenzodioxane PIM-1, J. Membr. Sci. 325 (2) (2008) 851–860.
[55] B. Tejerina, M.S. Gordon, Insertion Mechanism of N2 and O2 into T n (n= 8, 10, 12)-Silsesquioxane Framework, J. Phys. Chem. B 106 (45) (2002) 11764–11770.
[56] M. Tamaddondar, A.B. Foster, M. Carta, P. Gorgojo, N.B. McKeown, P.M. Budd, Mitigation of Physical Aging with Mixed Matrix Membranes Based on Cross-Linked PIM-1 Fillers and PIM-1, ACS Appl. Mater. Interfaces 12 (41) (2020) 46756–46766.
[57] H. Zhao, Q. Xie, X. Ding, J. Chen, M. Hua, X. Tan, Y. Zhang, High performance post-modified polymers of intrinsic microporosity (PIM-1) membranes based on multivalent metal ions for gas separation, J. Membr. Sci. 514 (2016) 305–312.
[58] Y.i. Li, T.-S. Chung, Molecular-level mixed matrix membranes comprising Pebax® and POSS for hydrogen purification via preferential CO2 removal, Int. J. Hydrogen Energy 35 (19) (2010) 10560–10568.
[59] A. Shariati, M. Omidkhah, M.Z. Pedram, New permeation models for nanocomposite polymeric membranes filled with nonporous particles, Chem. Eng. Res. Des. 90 (4) (2012) 563–575.
[60] L. Dong, M. Chen, J. Li, D. Shi, W. Dong, X. Li, Y. Bai, Metal-organic framework-graphene oxide composites: A facile method to highly improve the CO2 separation performance of mixed matrix membranes, J. Membr. Sci. 520 (2016) 801–811.
[61] G. Khanbabaei, E. Vasheghani-Farahani, A. Rahmatpour, Pure and mixed gas CH4 and n-C4H10 permeation in PDMS-fumed silica nanocomposite membranes, Chem. Eng. J. 191 (2012) 369–377.
[62] S.H. Pang, M.L. Jue, J. Leisen, C.W. Jones, R.P. Lively, PIM-1 as a Solution-Processable "Molecular Basket" for CO2 Capture from Dilute Sources, ACS Macro Lett. 4 (12) (2015) 1415–1419.
[63] F. Li, Y.i. Li, T.-S. Chung, S. Kawi, Facilitated transport by hybrid POSS®–Matrimid®–Zn2+ nanocomposite membranes for the separation of natural gas, J. Membr. Sci. 356 (1-2) (2010) 14–21.
[64] Y.i. Li, H.-M. Guan, T.-S. Chung, S. Kulprathipanja, Effects of novel silane modification of zeolite surface on polymer chain rigidification and partial pore blockage in polyethersulfone (PES)–zeolite A mixed matrix membranes, J. Membr. Sci. 275 (1-2) (2006) 17–28.
[65] S.D. Kelman, B.W. Rowe, C.W. Bielawski, S.J. Pas, A.J. Hill, D.R. Paul, B. D. Freeman, Crosslinking poly[1-(trimethylsilyl)-1-propyne] and its effect on physical stability, J. Membr. Sci. 320 (1-2) (2008) 123–134.
[66] N. Konnertz, Y.i. Ding, W.J. Harrison, P.M. Budd, A. Schönhals, M. Böhning, Molecular mobility and gas transport properties of nanocomposites based on PIM-1 and polyhedral oligomeric phenethyl-silsesquioxanes (POSS), J. Membr. Sci. 529 (2017) 274–285.
[67] K.L. Gleason, Z.P. Smith, Q. Liu, D.R. Paul, B.D. Freeman, Pure-and mixed-gas permeation of CO2 and CH4 in thermally rearranged polymers based on 3, 3′-dihydroxy-4, 4′-diamino-biphenyl (HAB) and 2, 2′-bis-(3, 4-dicarboxyphenyl) hexafluoropropane dianhydride (6FDA), J. Membr. Sci. 475 (2015) 204–214.
[68] P. Bernardo, F. Bazzarelli, F. Tasselli, G. Clarizia, C.R. Mason, L. Maynard-Atem, P. M. Budd, M. Lanč, K. Pilnáček, O. Vopička, K. Friess, D. Fritsch, Y.P. Yampolskii, V. Shantarovich, J.C. Jansen, Effect of physical aging on the gas transport and sorption in PIM-1 membranes, Polymer 113 (2017) 283–294.
[69] I. Borisov, D. Bakhtin, J. Luque-Alled, A. Rybakova, V. Makarova, A.B. Foster, W. J. Harrison, V. Volkov, V. Polevaya, P. Gorgojo, E. Prestat, P.M. Budd, A. Volkov, Synergistic enhancement of gas selectivity in thin film composite membranes of PIM-1, J. Mater. Chem. A 7 (11) (2019) 6417–6430.
[70] A.B. Foster, J.L. Beal, M. Tamaddondar, J.M. Luque-Alled, B. Robertson, M. Mathias, P. Gorgojo, P.M. Budd, Importance of small loops within PIM-1 topology on gas separation selectivity in thin film composite membranes, J. Mater. Chem. A 9 (38) (2021) 21807–21823.
[71] R.R. Tiwari, J. Jin, B.D. Freeman, D.R. Paul, Physical aging, CO2 sorption and plasticization in thin films of polymer with intrinsic microporosity (PIM-1), J. Membr. Sci. 537 (2017) 362–371.
[72] L.M. Robeson The upper bound revisited Journal of membrane science 320 1–2 2008 390 400.
[73] B. Comesaña-Gándara, J. Chen, C.G. Bezzu, M. Carta, I. Rose, M.-C. Ferrari, E. Esposito, A. Fuoco, J.C. Jansen, N.B. McKeown, Redefining the Robeson upper bounds for CO 2/CH 4 and CO 2/N 2 separations using a series of ultrapermeable benzotriptycene-based polymers of intrinsic microporosity, Energy Environ. Sci. 12 (9) (2019) 2733–2740.